Genesis and trends in marine heatwaves over the tropical Indian Ocean and their interaction with the Indian summer monsoon

J. S. Saranya[1,2], **M K Roxy**[1*], **Panini Dasgupta**[1,3] and **Ajay Anand**[1,4]

[1]*Centre for Climate Change Research, Indian Institute of Tropical Meteorology, Pune 411008, India*

[2]*College of Climate Change and Environmental Sciences, Kerala Agricultural University, Kerala, 680656, India*

[3]*Department of Meteorology and Oceanography, College of Science and Technology, Andhra University, Visakhapatnam, Andhra Pradesh 530003, India*

[4]*Department of Atmospheric Sciences, Cochin University of Science and Technology, Kerala, 682022, India*

Key points:

- An increasing trend in marine heatwaves is observed over the western Indian Ocean and the Bay of Bengal.
- Ocean warming and El Niño events drives the genesis and trends of marine heatwaves in the Indian Ocean.
- Marine heatwaves reduce the monsoon rainfall over the central Indian subcontinent while enhancing it over the southern peninsula.

JGR Oceans, submitted on 31 March 2021, last revised on 28 Oct 2021

*Corresponding author address: Roxy Mathew Koll, Indian Institute of Tropical Meteorology, Pune 411008, India. E-mail: roxy@tropmet.res.in

Abstract

Marine heatwaves (MHWs) are extreme oceanic warm water events (above 90th percentile threshold) that significantly impact the marine environment. Recent studies have explored the genesis and impacts of MHWs in the global oceans though they are least understood in the tropical Indian Ocean. Here we investigate the genesis and trend of MHWs in the Indian Ocean during 1982–2018 and their role in modulating the Indian monsoon. We find that the rapid warming in the Indian Ocean plays a critical role in increasing the number of MHWs. Meanwhile, the El Niño has a prominent influence on the occurrence of MHWs during the summer monsoon. The Indian Ocean warming and the El Niño variability have synergistically resulted in some of the strongest and long-lasting MHWs in the Indian Ocean.

The western Indian Ocean region experienced the largest increase in MHWs at a rate of 1.2–1.5 events per decade, followed by the north Bay of Bengal at a rate of 0.4–0.5 events per decade. Locally, the MHWs are induced by increased solar radiation, relaxation of winds, and reduced evaporative cooling. In the western Indian Ocean, the decreased winds further restrict the heat transport by ocean currents from the near-equatorial regions towards the north. Our analysis indicates that the MHWs in the western Indian Ocean and the north Bay of Bengal lead to a reduction in monsoon rainfall over the central Indian subcontinent. On the other hand, there is an enhancement of monsoon rainfall over southwest India due to the MHWs in the Bay of Bengal.

Plain Language Summary

Marine heatwaves are periods of extremely high temperatures in the ocean. Though recent studies have reported their occurrence and impacts in the global oceans, they are least understood in the tropical Indian Ocean. In the current study, we find that marine heatwaves are increasing in the Indian Ocean, with the largest increase observed over the western Indian Ocean, followed by the north Bay of Bengal. These marine heatwaves occur as a result of background ocean warming in the Indian Ocean and also in response to El Niño events in the Pacific Ocean. Locally, a peak in

solar radiation and a dip in evaporative cooling due to weak winds lead to the formation of these marine heatwaves. In the western Indian Ocean, the weak winds also reduce the heat transported by ocean currents from the near-equatorial regions towards the north, intensifying the marine heatwave. In turn, these marine heatwaves impact the monsoon by reducing the rainfall over the central Indian subcontinent while enhancing it over the southern peninsula.

1. Introduction

According to the Special Report on the Ocean and Cryosphere (SROCC) of the Intergovernmental Panel on Climate Change (IPCC), the global ocean will continue to warm during the 21st century (IPCC, 2019). By 2100, the ocean warming in the top 2000 m is estimated to be 5–7 times higher under the business-as-usual scenario and 2–4 times higher under the low emission scenario, relative to the temperature reported since 1970 (*very likely*). Under this warming scenario, a rise in extreme temperature events in the ocean is also projected. Marine heatwaves (MHWs) are anomalous warm water events in response to the warming ocean—defined when the daily sea surface temperature (SST) exceeds the 90th percentile for five or more days (percentile threshold may vary and can be as high as the 99th percentile) (Hobday et al., 2016, Schaeffer et al., 2017, Collins et al., 2019). MHWs are reported all over the world—the 2003 Mediterranean Sea MHW, 2011 West Australian MHW, 2013/15 Northeast Pacific MHW, 2015/16 Tasman Sea MHW are some of them. Numerous studies indicate that these anomalous temperature events can cause habitat destruction due to coral bleaching, seagrass destruction, and loss of kelp forests, affecting the fisheries sector adversely (Mills et al., 2013, Collins et al., 2019).

Numerous studies have focused on the mechanisms leading to the genesis of MHWs. Most of the MHWs in Indo-Pacific regions are associated with climate modes like the El Niño, the Indian Ocean Dipole (IOD), and the Pacific Decadal Oscillation (PDO). The 2014–2015 MHW in the Northeast Pacific was associated with the PDO and the North Pacific Gyre Oscillation (NPGO), though local and remote ocean-atmospheric processes enhanced the conditions that led to an

increase in SST in the Northeast Pacific (Bond et al., 2015, Joh and Lorenzo, 2017, Capotondi et al., 2019). Holbrook et al. (2019) suggested that the SST variability in the tropical Indian and Pacific oceans is related to the El Niño, IOD, and Indian Ocean warming.

Although several studies have explored the extreme temperature events in the Pacific and Atlantic oceans, there is hardly any in-depth research on MHWs in the Indian Ocean. In the southeast Indian Ocean, coral bleaching events due to the MHWs were reported, mostly associated with the El Niño and Madden-Julian Oscillations (MJO), riding over a global warming signal (Zhang et al., 2017). Studies have reported high SST conditions in the western Indian Ocean (Seychelles region), Arabian Sea, and the Bay of Bengal region (Andaman Sea) and also point out the coral bleaching events due to intense warming in these regions (Saji et al., 1999; Edward et al., 2018; Raj et al., 2018; Krishnan et al.,2011), suggesting that MHWs are behind these events.

The north Indian Ocean is a critical region because it supports large marine primary productivity, particularly during the South Asian summer monsoon (Roxy et al., 2016), and because of its role in modulating the intraseasonal and interannual variability of the monsoon (Roxy et al., 2007, 2012; Singh and Dasgupta 2017). Understanding the genesis and evolution of MHWs during the summer monsoon season and their changes due to ocean warming is hence crucial. In this study, for the first time, we explore the genesis and trend of MHWs in the Indian Ocean during the summer monsoon season (June–September). While many studies have addressed the impacts of MHWs on the marine ecosystem, there are hardly any studies investigating the impacts of MHWs on atmospheric circulation and rainfall. Hence, we investigate the interaction between MHWs and Indian summer monsoon circulation and rainfall.

2. Data and methods

2.1 Data

To identify the MHWs, we used the daily Optimum Interpolated Sea Surface Temperature (OISST) dataset at a resolution of 0.25° x 0.25°, for the period 1982–2018 (Reynolds et al., 2007).

In order to study the impact of MHWs on atmospheric conditions, we used the daily NOAA Interpolated Outgoing Longwave Radiation (OLR) measured from Advanced Very High-Resolution Radiometer (AVHRR) onboard NOAA polar-orbiting spacecraft (Liebmann and Smith, 1996), at a 2.5° x 2.5° resolution, for the period 1982–2018. The daily wind, latent heat flux, sensible heat flux, upward longwave radiation, downward solar radiation, surface net longwave radiation, and surface net solar radiation are obtained from the National Center for Environmental Prediction/National Centers for Atmospheric Research (NCEP/NCAR) reanalysis data at a resolution of 2.5° x 2.5° (Kalnay et al., 1996). For the analysis of the rainfall variability over India, we used the Indian Meteorological Department (IMD) daily rainfall at a resolution of 0.25° x 0.25° (Pai et al., 2014). All the analyses are compared with European Centre for Medium-Range Weather Forecasts (ECMWF) ERA5 reanalysis product (Hersbach and Dee, 2016). In the main text, we use NCEP/NCAR products, and in the supplementary information, we compare our results with ERA5 reanalysis products.

To investigate the ocean conditions during the MHWs, we obtained the ocean current data at 1/3° grid with a five-day temporal resolution from the Ocean Surface Current Analysis Real-time (OSCAR) (Dohan and Maximenko, 2010). The monthly potential temperature and salinity are obtained from ORAS4 at a horizontal resolution of 1°× 1° (Balmaseda et al., 2013). Apart from this, daily water temperature and salinity are obtained from the Hybrid Coordinate Ocean Model (HYCOM) reanalysis. We supplemented the heat budget analysis using the HYCOM reanalysis (Metzger et al., 2014) at a resolution of 1/12° for 1994–2015.

2.2 Methods

2.2.1 Detection of marine heatwaves

In this study, we identify MHWs from the OISST daily datasets, where the SST is above the 90th percentile (threshold) and persist for at least five days. Here, the 90th percentile and the baseline climatology of SST are calculated for each calendar day from the daily SSTs using an 11-day

window centered on that particular day of the year, across all years, within the climatology period (1982–2018)—and are smoothed using a 31-day moving average (Hobday et al. 2016, Oliver et al. 2018, Gupta et al. 2020). The reason for considering an 11-day window is to create enough sample size (407 samples vs. 37 samples) for estimating the climatology and the 90^{th} percentile at a daily timescale. This is important since due to day-to-day SST fluctuations, chances of a few outliers skewing the daily climatology or 90^{th} percentile values are high. The 31-day moving average is used to obtain a smoothed climatology that is seasonally varying and does not contain any higher-frequency variability than the seasonal timescale (below 30 days). This seasonally varying 90^{th} percentile will help us to identify the MHWs at any time of the year, regardless of the summer months (Oliver et al., 2018). We also utilize specific metrics to study and analyze the MHWs, such as the maximum intensity (maximum temperature anomaly during a particular MHW event), mean intensity (mean temperature anomaly during a specific MHW event), cumulative intensity (sum of temperature anomalies during a particular MHW event), duration (number of days between the starting and ending dates), and spatial extent (area covered by MHW event) (Hobday et al., 2016). To study the spatial extent of the MHWs, we counted the grids where the MHW events occurred and multiplied them by the grid area. To estimate the trend in MHWs, we used the OISST data from 1982–2018 and calculated MHW at each grid, and then fit a linear trend model. Along with the annual values, we also prepare the MHW metrics for June to September.

Further, we did a composite analysis of wind, SST, latent heat flux, sensible heat flux, upward longwave radiation, and downward solar radiation during one week before and after the starting date of MHW events. This provides us with a comprehensive picture of the genesis of MHWs and describes the physical and dynamical processes involved with the MHW genesis over the particular regions. To study the interaction between the MHWs and summer monsoon circulation and rainfall, we have included a composite analysis of wind at 850 hPa, OLR, omega at 500 hPa, vertically integrated moisture flux, and rainfall over India during the MHWs.

2.2.2 Mixed layer heat budget

To study the local factors influencing the genesis of MHWs, we estimated the mixed layer heat budget using the temperature tendency equation. The temperature tendency equation gives us a comprehensive picture of factors that lead to the change in the ocean surface temperature (Rodrigues et al., 2019). The temperature tendency equation is given by

$$\partial T_m/\partial t = -v.\nabla T_m + Q0/\rho C_p H_m + Res \quad (1)$$

where ρ is the density of seawater (1,026 kg m^{-3}), and C_p is the specific heat of seawater (3902 J kg^{-1} K^{-1}), and T_m is the mixed layer temperature. Here we have used the SST as a mixed layer temperature because the vertically averaged mixed layer temperature is close to the SST values (Foltz et al., 2003).

$\partial T_m/\partial t$ represents the rate of change of mixed layer temperature. The term -v.∇T indicates the advection and v indicate the horizontal velocity vector (v at 15m depth from OSCAR Ocean currents, vertically averaged over the mixed layer). H_m means the mixed layer depth (MLD) in meters. Using the monthly potential temperature and salinity data of ORAS4, we calculated the monthly MLD as the depth at which the density changes by a threshold of 0.05 kg m^{-3} for depth of 5 m. The monthly MLD is interpolated to daily to estimate the heat flux terms (Rodrigues et al., 2019).

$$Q_0 = Q_s + Q_b + Q_e + Q_h \quad (2)$$

Q_0 is the net surface heat flux (W m^{-2}), which includes the latent heat flux Q_e, and the sensible heat flux Q_h released from the ocean mixed layer, the net solar radiation received Q_s, and the net longwave radiation released Q_b. Finally, the *Res* include the remaining unresolved process, such as vertical diffusion, and entrainment. The heat budget analysis is also verified with HYCOM ocean current datasets. All the heat budget terms are calculated from 1994–2015 and averaged for the two study regions. Anomalies are derived from the 1994–2015 daily climatology. Then we

estimate the heat budget terms for the five days before the start date of MHWs in the selected regions.

3. Results

To investigate the changes in MHWs in the Indian Ocean, we first select those regions in the tropical Indian Ocean that experienced an increasing trend in MHWs during 1982–2018. The result section is organized into five sections. Section 3.1 describes the MHWs in the Indian Ocean and their trends. In section 3.2, we describe the seasonal climatology of MHWs for the regions where the trends are the largest. Section 3.3 addresses the role of dominant modes of climate variability on the MHWs in the tropical Indian Ocean. In section 3.4, we focus on the genesis and evolution of MHWs during the southwest monsoon season (June–September) and then describes the interaction between MHWs and the monsoon rainfall in section 3.5.

3.1 Observed trends in marine heat waves in the Indian Ocean

The climatological mean distribution of MHW frequency during 1982–2018 is shown in Figure 1a and b, indicating that MHWs are generally observed in the northern parts of north Indian Ocean. The trend in the annual MHW frequency from 1982–2018 over the Indian Ocean is shown in Figure 1c. The western Indian Ocean region (41°E–56°E, 8°S–8°N) shows the most prominent trend in MHWs, annually, though climatologically it was not a region with frequent MHWs. The western Indian Ocean region has an increasing trend of 1.2–1.5 MHW events per decade (p<0.01) at each grid point. The northern Arabian Sea also shows a similar increasing trend, though not well-defined. Meanwhile, in the eastern Indian Ocean and central equatorial Indian Ocean (80°E–110°E, 0°–20°S), the trend is about 0.4 MHW events per decade.

The boreal summer monsoon months (June–September) are immensely crucial for the Indian Ocean rim countries because the rainfall during this season supports the food, water, and energy security of this region (Beal et al., 2020; Wang et al., 2020). SST variability in the tropical

Indian Ocean regulates the monsoon circulation and rainfall. Recognizing the importance of the SSTs during the northern summer monsoon months, we investigate the changes in MHWs during this season (June–September), for 1982–2018 (Figure 1d). Climatologically, during this season, MHWs generally occur in the northern parts of the north Indian Ocean (Figure 1b). During June–September, there are two regions where MHWs activities are rapidly increasing, in terms of the frequency and the area covered. One is in the western Indian Ocean region, where the annual trend in MHWs frequency is also maximum. The second one is in the northern Bay of Bengal (85°E–93°E, 15°N–23°N) region, where a well-defined trend in MHW frequency is observed, at its maximum during the summer monsoon season (Figure 1d). These two regions are experiencing an increasing trend of 0.5 events per decade during June–September. Apart from these two locations, the coastal northeastern Arabian Sea also shows a similar increasing trend. Chatterjee et al. (2021) links these coastal Arabian Sea MHWs to the increase in the mean SST in the recent decades and the Indian Ocean basin-wide warming in response to El-Niño events during their decaying phase.

We further examine the month-wise trend of the frequency of MHWs over western Indian Ocean and northern Bay of Bengal region. For the western Indian Ocean region (in Figure 1e), we find that the increasing trend of MHW frequency is present in all months. The trend is highest during October to December, with the maximum in November. The trend in MHW frequency is moderate during February to May and August to September. For the north Bay of Bengal region, the MHWs frequency trends are small in January to April and November, while large in May to September, and moderate in October and December (Figure 1f). Notably, the western Indian Ocean region is crucial because it is experiencing a significant increasing trend in the frequency of MHWs year-round, while the north Bay of Bengal region is experiencing a significant trend during summer monsoon months.

Henceforth, we focus our analysis on the western Indian Ocean (41°E–56°E, 8°S–8°N) and north Bay of Bengal (85°E–93°E, 15°N–23°N) regions, where the MHW trends are the largest. We identified individual MHW events based on the spatial mean SST time series over western

Indian Ocean and north Bay of Bengal boxes in Figure 1d. There are 66 MHW events that occurred in the western Indian Ocean region during the 1982–2018 period, in which 21 events occurred during June–September. The north Bay of Bengal region witnessed 94 MHW events, and 34 out of these occurred during June–September. The time series of the annual and monsoon MHW frequency for western Indian Ocean and north Bay of Bengal are shown in Figure 1g, h. There is a significant rise in annual MHW frequency during 1982–2018 at a rate of 0.14 events per year for the western Indian Ocean and 0.09 events per year for the north Bay of Bengal. On the other hand, the MHW frequency during the monsoon season is increasing at a rate of 0.04 events per year in the western Indian Ocean region and 0.05 events per year in the north Bay of Bengal (Figure 1 g, h). It is evident from the time series that the trend of MHW frequency in the north Bay of Bengal during June–September shows higher values compared to the western Indian Ocean region during the same period.

3.2 Seasonal climatology of marine heatwaves in the tropical Indian Ocean

For the western Indian Ocean region, all the MHW metrics (except for the MHW events) show a double peak in the seasonal climatology signal during March and September months (Figure 2). During these two months, the duration of MHWs may reach 16 and 20 days, respectively. The mean intensity shows high seasonal variability. The mean intensity values during March and September are highest with mean values of 1.03°C and 1.1°C, respectively. In the case of maximum intensity, it is 1.3°C during the peak months. In the case of area covered by the MHW events, it is 1.4 million km^2 during the peak months of March and September. Meanwhile, the number of MHW events show peaks during the May, August, and October months.

MHWs in the north Bay of Bengal are short-lived, and the cumulative intensity and area covered are smaller compared to the western Indian Ocean. The duration and cumulative intensity of MHWS in the north Bay of Bengal do not exhibit large seasonal variations. The cumulative intensity, duration, and area exhibit a peak during April, while the peak in the mean intensity, and

maximum intensity is in May. Further, the number of events is maximum during May (14), June (14), and October (15) months. The cumulative intensity and duration in the peak month of April are 10°C days and 10 days, respectively. The mean intensity during the May month is 1.1°C, while the maximum intensity is 1.3°C. During April, the area is 0.4 million km^2.

3.3 Role of Indian Ocean warming and dominant modes of climate variability on marine heatwaves

Recent research on MHWs (Laufkötter, et al., 2020, Holbrook et al., 2019, Frölicher et al., 2018) and the IPCC SROCC point out that MHW events are a manifestation of the global warming trend (Collins et al., 2019). A pattern correlation between the tropical SST trends and tropical MHW trends shows a significantly high correlation (r=0.8 for annual values and r=0.6 for boreal summer season) supporting this argument. Besides the global SST rise, various modes of climate variability favor MHW events by generating the necessary background conditions (Holbrook et al., 2019).

This section investigates the role of different climate modes on the occurrences of MHW events, particularly the association with El Niño, Indian Ocean basin-wide warming mode (IOB, Indo-Pacific warming generally occurring during the post- El Niño periods), Indian Ocean Dipole (IOD), and the North Atlantic Oscillation (NAO). Figure 3 shows the number of MHW days coincident with these climate modes or overlapping modes. An active phase of a climate mode is defined when the corresponding climate indices have a value larger than its long-term standard deviation. Note that while classifying the association between MHWs and the climate modes, MHWs during co-occurring climate modes are not counted for individual modes. For example, MHW days that occur when positive IOD and negative NAO co-occur are not considered under either the individual positive IOD-only or negative NAO-only groups. The absence of any climate modes during the MHW is indicated as "Nil". It is important to note that the metric 'MHW days' is used instead of 'MHW events' for investigating the association between the MHWs and different climate modes. This is because a greater number of MHW events in a season or year does not

necessarily mean a correspondingly greater number of MHW days, as there may be a greater number of short MHW events in some years with short duration, and vice-versa.

Correlation and composite analysis of the yearly count of MHW days in the western Indian Ocean region with the annual mean SSTs show that these events are associated with the El Niño, IOB (Indian Ocean warming), and negative North Atlantic Oscillation (NAO) (Figure 3a, b). Out of all the western Indian Ocean MHW days, the most significant number of MHW days occur under the Indian Ocean warming condition (Figure 3a, b). There are a significant number of MHW days when no climate modes are present (Figure 3b, grey bar). Regardless, there are a large number of MHW days under the positive IOD and negative NAO conditions. The spatial correlation between the MHW days in the western Indian Ocean region and mean SSTs for June–September shows significant associations with warm SSTs in the western Indian Ocean and El Niño/IOD-like conditions (Figure 3c). The climate mode analysis shows that these MHW days occur either independent of the modes (Figure 3d, grey bar), or are associated with concurrent occurrences of positive IOD and negative NAO (Figure 3d, pink bar), positive IOD and El Niño (Figure 3d, dark-red bar) or during positive IOD only conditions, in that order. To summarize, Indian Ocean warming, El Niño, positive IOD, and negative NAO largely regulate the occurrence of MHWs in the western Indian Ocean.

Similar to the western Indian Ocean region, correlation and composite analysis of the yearly count of MHWs days in the north Bay of Bengal with the annual mean SST shows an association with the Indian Ocean warming, El Niño, and negative NAO (Figure 3e, f). Out of all the north Bay of Bengal MHW days, significant MHW days occur under the Indian Ocean warming condition. There are several MHW days associated with the negative NAO conditions following the IOB condition. Meanwhile, for June to September, the MHW days in the north Bay of Bengal appear to occur with warming in the north Indian Ocean (Figure 3g) and negative NAO pattern (Figure 3h).

In summary, occurrences of western Indian Ocean and north Bay of Bengal MHWs are more frequent while Indian Ocean warming is prominent basin wide (IOB) or when the western (for western Indian Ocean MHWs in summer) or northern (for Bay of Bengal MHWs in summer) exhibits warming. The western Indian Ocean SSTs also respond to the El Niño due to the subsidence of Walker circulation over these regions (Roxy et al. 2014, Xie et al., 2016). This subsidence inhibits deep convection and thereby suppresses the release of heat from the ocean to the atmosphere. Thus, the Indian Ocean attains its maximum temperatures under the IOB mode. That is, the background warming in the Indian Ocean has a strong influence on the MHWs in the Indian Ocean basin on an annual timescale. During a positive IOD event, the western Indian Ocean becomes warmer than its climatology (Murtugudde and Busalacchi, 1999; Saji et al., 1999). June–September MHWs in the western Indian Ocean region are often associated with these positive IODs (Holbrook et al., 2019). The negative NAO phases are also associated with MHWs over the north Bay of Bengal region. Holbrook et al. (2019) and Mishra et al. (2012) show an association between negative NAO and north Indian Ocean warming. However, the mechanism between the negative NAO and north Indian Ocean SSTs needed to be explored in detail. Though the occurrences of MHWs in the Indian Ocean exhibit potential association with the climate modes described here, we do not investigate the mechanisms through which their causal relationships are manifested.

3.4 Local ocean-atmospheric interaction leading to the genesis and evolution of MHW events

In this section we explore the role of local ocean-atmospheric conditions leading to the initiation and the persistence of MHWs in the Indian Ocean. It is observed that for the western Indian Ocean MHWs, the downward solar radiation leads the SST peak by ~10 days. However, this lead-lag relation is weak (r = 0.13). The increased downward solar radiation due to clear sky conditions may increase SST in the western Indian Ocean region but is not the primary reason for MHW genesis. Meanwhile, the reduced wind speed and evaporation (denoted by the negative wind

anomaly and reduced upward latent heat flux anomaly in Figure 4b) leads the SST anomalies by ~3 days (r = -0.24, p < 0.05), assisting the MHW formation. Besides the air-sea fluxes, reduced wind speed also impacts the ocean current over the western Indian Ocean Region. The ocean currents in the western Indian Ocean region (driven by strong cross-equatorial monsoon winds) are usually strong and transport heat away from the equator. Hence, a weakening of the cross-equatorial winds can potentially reduce ocean heat transport by accumulating the heat in this region, enhancing the MHWs.

To comprehend the spatial distribution of the lead-lag relationship, composites of different variables from ten days before and after the MHW genesis date are presented in Figure 4b. The SST anomalies show a dipole pattern with cold anomalies at 15°N and warm anomalies at the equator prior to the genesis of western Indian Ocean MHWs. In Figure 4a, the region of cold SST anomalies can be observed north of the western Indian Ocean region ten days prior to the MHWs initiation. The warm SST anomalies near the equator gradually become prominent as the MHW initiates. Interestingly, the cold SST anomalies (up to -0.5° C) at the north of the western Indian Ocean region is maintained consistently from about a month (30 days) to almost a week (6 days) prior to the MHWs genesis. The meridional SST difference between the north (15°N) and western Indian Ocean region is also maintained during the same period prior to the genesis of MHWs (supplementary information Figure S4c, d). These cold SST anomalies at 15°N and the meridional SST difference may have a significant role in reducing the strength of cross-equatorial wind flow (Figure 4b and supplementary information S4). The reduced wind speed (up to -1 m/s during the pentad leading to the MHW onset) not only reduces the air-sea fluxes (reduce evaporation) (Figure 4b and supplementary information S4) but also affects the strength of ocean currents, leading to decreased heat transport from the equator towards the north. These factors contribute to the MHW formation in the particular region. Ten days prior to the MHWs genesis, the clear sky condition over the western Indian Ocean region due to the weak cross-equatorial flow and less evaporation increases downward solar radiation. The increase in downward solar radiation further increases

337 the SST. Therefore, from the lead-lag time series and the spatial composites, we identify the role
338 of reduced heat transport, decreased evaporation from the ocean surface, and increased downward
339 short-wave radiation behind the MHWs genesis over the western Indian Ocean region. We find
340 the release of upward sensible heat flux and latent heat flux from the ocean after 3–5 days of the
341 MHWs genesis reduce the ocean temperature and thereby the MHW intensity.

342 To explore the ocean dynamics involved in the genesis of MHWs over the western Indian
343 Ocean region, we performed an oceanic mixed layer heat budget analysis (Figure 6 a, b, c). We
344 calculated the composites of the heat budget terms for the five days before the onset of MHWs (5-
345 day average). The heat budget analysis is carried out for the MHWs between 1994–2015, based
346 on the availability of ocean potential temperature and salinity data. Figure 6a, b shows the role of
347 the advection terms and the heat flux terms on the rate of change of SST in the western Indian
348 Ocean region. In the advection term, the heat transport by the zonal ocean currents (the zonal
349 advection term) is dominant compared to the meridional component.

350 In comparison to the advection term, the heat flux term is found to be contributing more to
351 the temperature change. In the net heat flux term, the net solar radiation received in the mixed
352 layer and the latent heat stored (due to less evaporation) in the mixed layer are the major
353 contributors. The solar heating of the ocean surface and decreased evaporative cooling favors the
354 genesis of MHWs in the western Indian Ocean region. The time-integrated heat budget terms in
355 Figure 6c reveal the time evolution of different heat budget parameters.

356 In the north Bay of Bengal region, reduced wind speed anomalies and evaporation lead the
357 MHWs genesis by ~2 days (r=-0.38) (Figure 5a). Due to weakened wind speed, evaporative
358 cooling over the ocean surface becomes less, and hence the SST increases. An increased OLR and
359 downward solar radiation lead SST by ~4 days with r values 0.28 and 0.31, respectively. Hence,
360 the reduced evaporative cooling and increased incoming solar insolation (clear sky conditions)
361 jointly raise the SSTs over the north Bay of Bengal region leading to the MHWs. From the spatial
362 composites in Figure 5b, the SST shows a rapid increase coinciding with the MHW genesis day.

It is seen that the northeasterly winds establish in the north Bay of Bengal region 5 days before the onset of MHW and weaken the southwesterlies over the particular region. This reduced wind speed leads to a decrease in evaporation at the ocean surface, in turn reducing the release of upward latent heat flux from the ocean. A negative latent heat flux anomaly in the north Bay of Bengal region is observed 5 days before the onset of MHWs, confirming these results. Moreover, there is an increased downward solar radiation and increased OLR five days before the genesis of MHWs, peaking on the starting day of MHWs. We can infer that the decreased upward latent heat flux due to the decreased wind speed and the clear sky condition (increased downward short-wave radiation) contribute to the MHW genesis in the north Bay of Bengal region. After 3 days of the MHW genesis, there is a release of sensible heat and upward longwave radiation from the ocean, reducing the ocean temperature and helping terminate MHWs events.

It is worth noting that (Figures 6d, e, f) in the northern Bay of Bengal, the temperature change is mainly attributed to the net heat flux, and there is less contribution from the heat advection term. The latent heat (due to decreased evaporation) and net solar radiation have a prominent role among the heat flux terms. Meanwhile, the role of advection is minimal here. In a nutshell, it can be inferred that the weak wind causes decreased evaporative cooling of the ocean, while the increased solar heating is also accompanying the temperature rise in this region. Figure 6f represents the time-integrated heat budget terms. It is evident that for the north Bay of Bengal region, the MHW duration is comparatively less than the western Indian Ocean region. In summary, the role of reduced wind speed and evaporation is more prominent in north Bay of Bengal MHWs, than the western Indian Ocean MHWs.

The lead-lag and heat budget analysis here using NCEP reanalysis are cross-validated using ERA5 reanalysis products in the supplementary information (Figure S2 & S3). In the lead-lag analysis the ERA5 and NCEP show similar results. The significant lead-lag correlations of both the dataset are similar, which supports the proposed lead-lag relation of SST and other atmospheric conditions, except the correlation with OLR. In case of heat budget analysis, the ERA5 (Figure

S5) and the NCEP (Figure 6) show a similar conclusion, indicating that the downward solar radiation and latent heat fluxes contribute largely to the peak in SST. However, there are some disagreements also. For example, in the western Indian Ocean region, the ERA5 indicates that the temperature advection by ocean currents is a larger contributor than the net heat flux (Figure S5a&b). Also, for the both regions, the downward solar radiation and latent heat fluxes are large in the ERA5 (Figure S5) as compared to the NCEP (Figure 6) reanalysis. The differences in the heat flux terms contribution may be due to the nature of the reanalysis products.

3.5 Interaction of marine heatwaves with the Indian summer monsoon

The analysis in this section is focused on the summer monsoon rainfall variations during the MHWs over both the western Indian Ocean and north Bay of Bengal regions. We analyzed the mean pattern of SST, vertical velocity (omega at 500 hPa), wind (at 850 hPa), OLR, and vertically integrated moisture flux and the rainfall. It is fascinating that the MHWs over the two regions have the opposite impacts on Indian summer monsoon rainfall.

The SST anomaly composite during western Indian Ocean MHWs shows a warming pattern in this region. The SST anomalies vary from 0.9°C–1.2°C (Figure 7a). Moreover, negative omega (vertical velocity) anomalies at 500 hPa and OLR confirm enhanced convective activity during MHW days over the western Indian Ocean MHW region. Higher SST triggers the ascending motion of air and convection (Figure 7c, Figure S6a). At the same time, the circulation pattern shows strong northeasterly wind anomalies, indicating that the mean southwesterly monsoon winds are weak during this time (Figure S6a). The anomalous Hadley circulation during western Indian Ocean MHW events shows increased convective activities over the equatorial Indian Ocean, while the descending branch occurs over the Indian subcontinent (Figure 7g). This indicates that the western Indian Ocean MHWs are conducive for inducing dry conditions over the Indian landmass. The vertically integrated moisture flux divergence analysis contributes a more precise picture, suggesting an anomalous moisture flux divergence over the Indian subcontinent,

with the moisture transported away towards the western Indian Ocean region (Figure 7e). The mean pattern of rainfall over Indian landmass agrees with the results, with reduced rainfall across most of the subcontinent where the monsoon westerlies are prominent (Figure 7i).

In Figure 7b, the higher SST anomalies in the north Bay of Bengal region are apparent during June–September MHWs. The positive omega anomalies at 500 hPa and the positive OLR values imply dry subsidence and absence of cloud cover (clear sky condition) in this region during strong MHW events (Figure 7d, Figure S6b). However, negative OLR anomalies (above -15W m^{-2}) and negative omega anomalies at 500 hPa level over the western India and adjacent ocean region suggest enhanced convection and strong ascending motion in these regions. The vertically integrated moisture flux anomalies (Figure7f) indicate a convergence of the wind in the same region where the OLR and omega anomalies are negative.

Figure 7h shows the mean meridional circulation averaged over the 41°E–100°E for the north Bay of Bengal region during the June–September MHW days for the period 1982–2018. Over the southern part of the Indian subcontinent (0–15°N), there is increased convection during MHW days, supporting the previous results that show an increased convection in the vertical velocity over the region, while there is a suppressed convection at the 20°N due to the dry subsidence over north Bay of Bengal. We find an anomalous moisture flux convergence over the Indian landmass and anomalous moisture flux divergence over the north Bay of Bengal, which provides the cause for the observed rainfall pattern. The moisture transport from the warm north Bay of Bengal region by the anomalous easterly winds plays a crucial role in enhancing the rainfall over the south peninsular Indian subcontinent. There is a convergence of southwesterly monsoon winds and anomalous easterly winds from the Bay of Bengal at 850 hPa over the south-west Indian subcontinent (Figure S6b). The moisture convergence introduces the convective instability over this region. To summarize, there is a significant relationship between the MHWs in the northern Bay of Bengal and increased summer monsoon rainfall over southwest India.

3.5 Conclusion

Here we have conducted a detailed investigation of the trends and genesis of MHW events in the tropical Indian Ocean—and its interaction with the Indian summer monsoon. We find that the trend in annual frequency of MHWs is relatively higher in the western equatorial Indian Ocean (41°E–56°E, 8°S–8°N), which experienced 66 events during the 1982–2018 periods. We further studied the trend in MHW frequency during the Indian summer monsoon period (June–September) and find that the trend in MHWs is prominent in the western Indian Ocean and the north Bay of Bengal (85°E–93°E, 15°N–23°N). The north Bay of Bengal experienced 94 MHW events, wherein 34 events occurred from June to September, while in the western Indian Ocean region, it was 21 events.

We further investigate the climate modes driving the MHWs over these two regions. It is observed that the long-term persistence of MHWs in the western Indian Ocean region is associated with the background SST warming primarily identified with the Indian Ocean basin-wide warming (IOB) and also the El Niño, IOD, and NAO. Roxy et al. (2014) and Abish et al. (2018) show that the western Indian Ocean is warming at a rapid pace since the 1950s, largely in response to anthropogenic warming but manifested through an asymmetry in the ENSO impact—whereby El Niño events cause anomalous warming in the western Indian Ocean and La Niña events fail to cool the region. They also found that the ENSO events are more intense in the recent decades and this result in a positive SST skewness. Han et al. (2010) identifies a change in the local Hardly and Walker circulation that affect the distribution of sea level and temperature in the in the Indian Ocean, with an increase in the western Indian Ocean. Regardless, the role of mean SST rise in the western Indian Ocean is obvious (Roxy et al., 2020). Figure S7 shows an increase in the SST in the western Indian Ocean after year 2000 (both for annual and June-September) in comparison with pre-2000 period, indicating the role of background warming on the increase in MHWs in the western Indian Ocean. The background warming and the MHWs potentially decrease the summer

monsoon rainfall over the central and north east India post-2000, as observed by the rainfall difference between the two periods (Figure S7c).

For the north Bay of Bengal MHWs, the longer duration of these events is linked to the IOB, El Niño, and NAO. Earlier studies have pointed out that El Niño, IOD and IOB are major contributors to anomalous warm SST events in the tropical ocean (Holbrook et al., 2019). Notably, the SST trend due to global warming is manifested through the increased number of MHW events.

We investigated the seasonal climatology of MHW metrics in both the selected regions. For the western Indian Ocean region, it is found that all the MHWs metrics (except for the MHW events) have a double peak in the seasonal climatology during March and September months. The highest number of western Indian Ocean MHW events occur during May, August, and October. As compared to the MHWs in the western Indian Ocean, the MHWs in the north Bay of Bengal are short-lived, and the cumulative intensity and the area covered are smaller. The MHWs in the north Bay of Bengal do not exhibit large seasonal variation in the duration and cumulative intensity. The highest number of north Bay of Bengal MHWs events occur during May, June, and October months (14, 14 and 15 events, respectively). Interestingly, these months (May, early June, and October) are when the cyclones are active in the Bay of Bengal. Warm SSTs set an ideal precondition for cyclones, and it is hence necessary to closely monitor the basin to understand how these MHWs are interacting with the cyclones.

Focusing on the factors influencing the genesis of MHWs events in the tropical Indian Ocean, the results here show that in the western Indian Ocean region, MHWs are formed due to a relaxation of winds prior to the event. This tranquility in the winds is making the SST rise through two ways—through a decrease in the evaporative cooling at the ocean surface, and through a weakened transport of the heat by ocean currents. Apart from this, increased solar heating of the ocean surface due to reduced cloud cover also helps the formation of a warm pool in the western Indian Ocean region. We find that solar insolation plays a major role in MHW genesis from ocean mixed layer heat budget analysis. The reduced upward latent heat flux and zonal heat advection

are the other major contributors. Interestingly, we observe an occurrence of cold SST (north of the western Indian Ocean region) region 35~40 days prior to western Indian Ocean MHWs and a relatively low SST gradient. This low SST gradient and cold pool may be the reason for the weakening of cross-equatorial flow. The genesis of MHWs in the Tasman Sea and China's marginal seas also had a similar role in ocean dynamics (Oliver et al., 2017, Yao et al., 2020).

For the north Bay of Bengal region, it is observed that the reduction in wind speed and thereby reduction in the release of latent heat is one of the major causes for MHW genesis. Along with this, the increased solar radiation at the ocean surface also plays a key role. However, unlike the western Indian Ocean region, the signature of heat advection behind the genesis of MHWs is absent in the case of the north Bay of Bengal. In this study, we find that the western Indian Ocean MHWs have a longer persistence time, and the process of genesis is also slower than the MHWs in the north Bay of Bengal.

The MHWs in the western Indian Ocean and the north Bay of Bengal have strong links to the observed variability of the Indian summer monsoon rainfall. We find that both the MHWs are associated with the drying conditions over the central Indian subcontinent. However, there is a significant increase in the rainfall over south peninsular India in response to the MHWs in the north Bay of Bengal. Climate model projections suggest further warming of the Indian Ocean in the future, which will very likely intensify the MHWs (Collins et al., 2019) and their impact on the monsoon rainfall. Since the frequency, intensity, and area of marine heatwaves are increasing, it is essential that we closely monitor and forecast these events in advance in order to mitigate their impacts.

Acknowledgments

The Optimum Interpolated Sea Surface Temperature (OISST) and the Outgoing Longwave Radiation (OLR) are available from National Oceanic and Atmospheric Administration (NOAA) (Reynolds et al., 2007). The daily wind, latent heat flux, sensible heat flux, upward longwave

radiation, downward solar radiation, surface net longwave radiation, and surface net solar radiation are available from the National Center for Environmental Prediction/National Centers for Atmospheric Research (NCEP/NCAR) reanalysis data (Kalnay et al., 1996). For the analysis of the rainfall variability over the India, we used daily rainfall available from the Indian Meteorological Department (Pai et al., 2014). The ocean current data is available from the Ocean Surface Current Analysis Real-time (OSCAR), provided by the Earth Space Research (Dohan and Maximenko, 2010). J.S.S. acknowledges the support of Dr. P. O. Nameer, Dean of College of Climate Change and Environmental Sciences (CCES) and Dr. M. Rajeevan, Secretary to the Ministry of Earth Sciences (MoES), for supporting her visit to the Indian Institute of Tropical Meteorology (IITM).

Author contributions

M.K.R. conceived the study and J.S.S. performed the analysis. J.S.S., M.K.R., and P.D. contributed to the interpretation of the results and drafting of the manuscript for publication. A.A. performed some of the preliminary analysis.

References

Abish, B., Cherchi, A. and Ratna, S.B., 2018. ENSO and the recent warming of the Indian Ocean. Int. *J. Climatol.*, 38(1), pp.203-214.

Balmaseda, M.A., Trenberth, K.E., Källén, E (2013), Distinctive climate signals in reanalysis of global ocean heat content, *Geophys. Res. Lett.*, 40, 1754–1759, doi:1002/grl.50382.

Beal, L.M., Vialard, J., Roxy, M.K., Li, J., Andres, M., Annamalai, H., Feng, M., Han, W., Hood, R., Lee, T. and Lengaigne, M., 2020. A Road Map to IndOOS-2: Better Observations of the Rapidly Warming Indian Ocean. *Bull. Am. Meteorol. Soc*., 101(11), pp.E1891-E1913.

Benthuysen, J.A., Tonin, H., Brinkman, R., Herzfeld, M., Steinberg, C (2016), Intrusive upwelling in the Central Great Barrier Reef, *J. Geophys. Res. Oceans*, 121, 8395–8416, doi:10.1002/2016JC012294.

Bond, N. A., Cronin, M. F., Freeland, H., & Mantua, N. (2015). Causes and impacts of the 2014 warm anomaly in the NE Pacific. *Geophys. Res. Lett.*, 42(9), 3414-3420.

Capotondi, A., Sardeshmukh, P. D., Di Lorenzo, E., Subramanian, A. C., & Miller, A. J. (2019). Predictability of US West Coast Ocean Temperatures is not solely due to ENSO. *Sci. Rep.*, 9(1), 1-10.

Chatterjee, A., G. Anil, and L. R. Shenoy, 2021: Marine Heatwaves in the Arabian Sea. *Ocean Sci. Discuss.*, 1-27.

Chen, K., Gawarkiewicz, G., Kwon, Y.O., and Zhang, W.G. (2015), The role of atmospheric forcing versus ocean advection during the extreme warming of the Northeast US continental shelf in 2012, *J.Geophys. Res. Oceans*, 120(6), 4324-4339.

Collins M., M. Sutherland, L. Bouwer, S.-M. Cheong, T. Frölicher, H. Jacot Des Combes, M.K. Roxy, I. Losada, K. McInnes, B. Ratter, E. Rivera-Arriaga, R.D. Susanto, D. Swingedouw, and L. Tibig, 2019: Extremes, Abrupt Changes and Managing Risk. In: IPCC Special Report on the Ocean and Cryosphere in a Changing Climate [H.-O. Pörtner, D.C. Roberts, V. Masson-Delmotte, P. Zhai, M. Tignor, E. Poloczanska, K. Mintenbeck, A. Alegría, M. Nicolai, A. Okem, J. Petzold, B. Rama, N.M. Weyer (eds.)].

Darmaraki, S., Somot, S., Sevault, F., Nabat, P., Cabos Narvaez, W.D., Cavicchia, L., Djurdjevic, V., Li, L., Sannino, G., Sein, D.V (2019), Future evolution of Marine Heatwaves in the Mediterranean Sea, *Clim. Dyn*., 53, 1371–1392, doi:10.1007/s00382-019-04661-z.

Dohan, K., Maximenko, N (2010), Monitoring Ocean Currents with Satellite Sensors, *Oceanography*, 23, 94–103, doi:10.5670/oceanog.2010.08.

Edward, J.P., Mathews, G., Raj, K.D., Laju, R.L., Bharath, M.S., Arasamuthu, A., Kumar, P.D., Bilgi, D.S. and Malleshappa, H., 2018. Coral mortality in the Gulf of Mannar, southeastern India, due to bleaching caused by elevated sea temperature in. *Curr. Sci*., 114(9), p.1967.

Elzahaby, Y., Schaeffer, A (2019), Observational Insight Into the Subsurface Anomalies of Marine Heatwaves, *Front. Mar. Sci.*, 6, doi:10.3389/fmars.2019.00745.

Foltz, G.R., Grodsky, S.A., Carton, J.A. and McPhaden, M.J., 2003. Seasonal mixed layer heat budget of the tropical Atlantic Ocean. *J. Geophys. Res. Oceans*, 108(C5).

Frölicher, T.L (2019), Chapter 5 - Extreme climatic events in the ocean, in: Cisneros-Montemayor, A.M., Cheung, W.W.L., Ota, Y. (Eds.), Predicting Future Oceans, *Elsevier*, 53–60, doi:10.1016/B978-0-12-817945-1.00005-8.

Frölicher, T.L., Fischer, E.M., Gruber, N, (2018), Marine heatwaves under global warming, *Nature*, 560, 360–364, doi:10.1038/s41586-018-0383-9.

Gupta, A. S, Thomsen, M., Benthuysen, J.A. et al. Drivers and impacts of the most extreme marine heatwave events. *Sci. Rep.*, 10, 19359 (2020).

Hersbach, H. and Dee, D.J.E.N., 2016. ERA5 reanalysis is in production. *ECMWF newsletter*, 147(7), pp.5-6.

Hobday, A.J., Alexander, L.V., Perkins, S.E., Smale, D.A., Straub, S.C., Oliver, E.C.J., Benthuysen, J.A., Burrows, M.T., Donat, M.G., Feng, M., Holbrook, N.J., Moore, P.J., Scannell, H.A., Gupta, A.S., Wernberg, T (2016), A hierarchical approach to defining marine heatwaves, *Prog. Oceanogr*., 141, 227–238, doi:10.1016/j.pocean.2015.12.014.

Holbrook, N.J., Scannell, H.A., Gupta, A.S., Benthuysen, J.A., Feng, M., Oliver, E.C.J., Alexander, L.V., Burrows, M.T., Donat, M.G., Hobday, A.J., Moore, P.J., Perkins-Kirkpatrick, S.E., Smale, D.A., Straub, S.C., Wernberg, T (2019), A global assessment of marine heatwaves and their drivers, *Nat. Commun*., 10, 1–13, doi:10.1038/s41467-019-10206-z.

IPCC, 2019: IPCC Special Report on the Ocean and Cryosphere in a Changing Climate [H.-O. Pörtner, D.C. Roberts, V. Masson-Delmotte, P. Zhai, M. Tignor, E. Poloczanska, K. Mintenbeck, A. Alegría, M. Nicolai, A. Okem, J. Petzold, B. Rama, N.M. Weyer (eds.)].

Jackson, J.M., Johnson, G.C., Dosser, H.V., Ross, T (2018), Warming From Recent Marine Heatwave Lingers in Deep British Columbia Fjord, *Geophys. Res. Lett*., 45, 9757–9764, doi:10.1029/2018GL078971.

Joh, Y., Lorenzo, E.D (2017), Increasing Coupling Between NPGO and PDO Leads to Prolonged Marine Heatwaves in the Northeast Pacific, *Geophys. Res. Lett*., 44, 11,663-11,671, doi:10.1002/2017GL075930.

Kalnay, E., Kanamitsu, M., Kistler, R., Collins, W., Deaven, D., Gandin, L., Iredell, M., Saha, S., White, G., Woollen, J. and Zhu, Y., 1996. The NCEP/NCAR 40-year reanalysis project. *Bull. Amer. Meteor*., 77(3), pp.437-472.

Krishnan, P., Roy, S.D., George, G., Srivastava, R.C., Anand, A., Murugesan, S., Kaliyamoorthy, M., Vikas, N., Soundararajan, R (2011), Elevated sea surface temperature during May 2010 induces mass bleaching of corals in the Andaman, *Curr. Sci.*, 100, 111–117.

Laufkötter, C., Zscheischler, J. and Frölicher, T.L., 2020. High-impact marine heatwaves attributable to human-induced global warming. *Science*, 369(6511), pp.1621-1625.

Liebmann, B., & Smith, C. A. (1996). Description of a complete (interpolated) outgoing longwave radiation dataset. *Bull. Am. Meteorol. Soc*., 77(6), 1275-1277.

Metzger, E.J., Smedstad, O.M., Thoppil, P.G., Hurlburt, H.E., Cummings, J.A., Wallcraft, A.J., Zamudio, L., Franklin, D.S., Posey, P.G., Phelps, M.W. and Hogan, P.J., 2014. US Navy operational global ocean and Arctic ice prediction systems. *Oceanography*, 27(3), pp.32-43.

Mills, K.E., Pershing, A.J., Brown, C.J., Chen, Y., Chiang, F.-S., Holland, D.S., Lehutha, S., Nye, J.A., Sun, J.C., Thomas, A.C., Wahle, R.A (2013), Fisheries Management in a Changing Climate: Lessons from the 2012 Ocean Heat Wave in the Northwest Atlantic, *Oceanography*, 26, 191–195.

Mishra, V., Smoliak, B.V., Lettenmaier, D.P. and Wallace, J.M., 2012. A prominent pattern of year-to-year variability in Indian Summer Monsoon Rainfall. *Proc. Natl. Acad. Sci.* U.S.A, 109(19), pp.7213-7217.

Murtugudde, R., and Busalacchi, A. J. (1999). Interannual variability of the dynamics and thermodynamics of the tropical Indian Ocean. *Journal of Climate*, 12(8), 2300-2326.

Oliver, E.C., Benthuysen, J.A., Bindoff, N.L., Hobday, A.J., Holbrook, N.J., Mundy, C.N., and Perkins-Kirkpatrick, S.E (2017), The unprecedented 2015/16 Tasman Sea marine heatwave, *Nat.Commun*., 8(1), 1-12.

Oliver, E.C., Burrows, M.T., Donat, M.G., Gupta, A.S., Alexander, L.V., Perkins-Kirkpatrick, S.E., Benthuysen, J., Hobday, A.J., Holbrook, N.J., Moore, P.J. and Thomsen, M.S., 2019. Projected marine heatwaves in the 21st century and the potential for ecological impact. *Front. Mar. Sci.* 6, p.734.

Oliver, E.C.J., Donat, M.G., Burrows, M.T., Moore, P.J., Smale, D.A., Alexander, L.V., Benthuysen, J.A., Feng, M., Gupta, A.S., Hobday, A.J., Holbrook, N.J., Perkins-Kirkpatrick, S.E., Scannell, H.A., Straub, S.C., Wernberg, T. 2018a , Longer and more

frequent marine heatwaves over the past century, *Nat. Commun*., 9, 1–12, doi: 10.1038/s41467-018-03732-9.

Pai, D.S., Sridhar, L., Rajeevan, M., Sreejith, O.P., Satbhai, N.S. and Mukhopadhyay, B., 2014. Development of a new high spatial resolution (0.25× 0.25) long period (1901–2010) daily gridded rainfall data set over India and its comparison with existing data sets over the region. *Mausam*, 65(1), pp.1-18.

Piatt, J.F., Parrish, J.K., Renner, H.M., Schoen, S.K., Jones, T.T., Arimitsu, M.L., Kuletz, K.J., Bodenstein, B., García-Reyes, M., Duerr, R.S., Corcoran, R.M., Kaler, R.S.A., McChesney, G.J., Golightly, R.T., Coletti, H.A., Suryan, R.M., Burgess, H.K., Lindsey, J., Lindquist, K., Warzybok, P.M., Jahncke, J., Roletto, J., Sydeman, W.J (2020), Extreme mortality and reproductive failure of common murres resulting from the northeast Pacific marine heatwave of 2014-2016, *PLOS ONE 15*, e0226087, doi:10.1371/journal.pone.0226087.

Raj, K.D., Mathews, G., Bharath, M.S., Laju, R.L., Kumar, P.D., Arasamuthu, A. and Edward, J.P., 2018. Cushion star (Culcitaschmideliana) preys on coral polyps in Gulf of Mannar, Southeast India. *Mar Freshw Behav Physiol*, 51(2), pp.125-129.

Rodrigues, R.R., Taschetto, A.S., Gupta, A.S., Foltz, G.R (2019), Common cause for severe droughts in South America and marine heatwaves in the South Atlantic, *Nat. Geosci*., 12, 620–626, doi:10.1038/s41561-019-0393-8.

Roxy, M.K., Modi, A., Murtugudde, R., Valsala, V., Panickal, S., Prasanna Kumar, S., Ravichandran, M., Vichi, M. and Lévy, M., 2016. A reduction in marine primary productivity driven by rapid warming over the tropical Indian Ocean. *Geophys. Res. Lett*., 43(2), pp.826-833.

Roxy, M.K., Ritika, K., Terray, P., Masson, S (2014), The Curious Case of Indian Ocean Warming, *J. Clim*., 27, 8501–8509, doi:10.1175/JCLI-D-14-00471.1.

Roxy, M.K., Ritika, K., Terray, P., Murtugudde, R., Ashok, K., Goswami, B.N (2015), Drying of Indian subcontinent by rapid Indian Ocean warming and a weakening land-sea thermal gradient, *Nat. Commun*., 6, 1–10, doi:10.1038/ncomms8423.

Roxy, M. and Tanimoto, Y., 2012. Influence of sea surface temperature on the intraseasonal variability of the South China Sea summer monsoon. *Clim. Dyn*., 39(5), pp.1209-1218.

Saji, N.H., Goswami, B.N., Vinayachandran, P.N. and Yamagata, T., 1999. A dipole mode in the tropical Indian Ocean. *Nature*, 401(6751), pp.360-363.

Schaeffer, A., Gramoulle, A., Roughan, M., Mantovanelli, A (2017), Characterizing frontal eddies along the East Australian Current from HF radar observations, *J. Geophys. Res. Oceans*, 122, 3964–3980, doi:10.1002/2016JC012171.

Schlegel, R.W., Oliver, E.C.J., Wernberg, T., Smit, A.J (2017), Nearshore and offshore co-occurrence of marine heatwaves and cold-spells, *Prog. Oceanogr*., 151, 189–205, doi:10.1016/j.pocean.2017.01.004.

Singh, C. and Dasgupta, P., 2017. Unraveling the spatio-temporal structure of the atmospheric and oceanic intra-seasonal oscillations during the contrasting monsoon seasons. *Atmos. Res*., 192, pp.48-57.

674 Walker, H.J., Hastings, P.A., Hyde, J.R., Lea, R.N., Snodgrass, O.E., Bellquist, L.F (2020),
675 Unusual occurrences of fishes in the Southern California Current System during the warm
676 water period of 2014–2018, *Estuar. Coast. Shelf Sci*., 236, 106634,
677 doi:10.1016/j.ecss.2020.106634.

678 Wang, B., Biasutti, M., Byrne, M.P., Castro, C., Chang, C.P., Cook, K., Fu, R., Grimm, A.M., Ha,
679 K.J., Hendon, H. and Kitoh, A., 2020. Monsoons Climate Change Assessment. *Bull. Am.*
680 *Meteorol. Soc.*

681 Xie, S.P., Kosaka, Y., Du, Y., Hu, K., Chowdary, J.S. and Huang, G., 2016. Indo-western Pacific
682 ocean capacitor and coherent climate anomalies in post-ENSO summer: A review. *Adv.*
683 *Atmos. Sci.*, 33(4), pp.411-432.

684 Yao, Y., Wang, J., Yin, J., Zou, X (2020), Marine Heatwaves in China's Marginal Seas and
685 Adjacent Offshore Waters: Past, Present, and Future, *J. Geophys. Res. Oceans*, 125,
686 e2019JC015801, doi:10.1029/2019JC015801.

687 Zhang, N., Feng, M., Hendon, H.H., Hobday, A.J., Zinke, J (2017), Opposite polarities of ENSO
688 drive distinct patterns of coral bleaching potentials in the southeast Indian Ocean, *Sci. Rep.*,
689 7, doi:10.1038/s41598-017-02688-y.

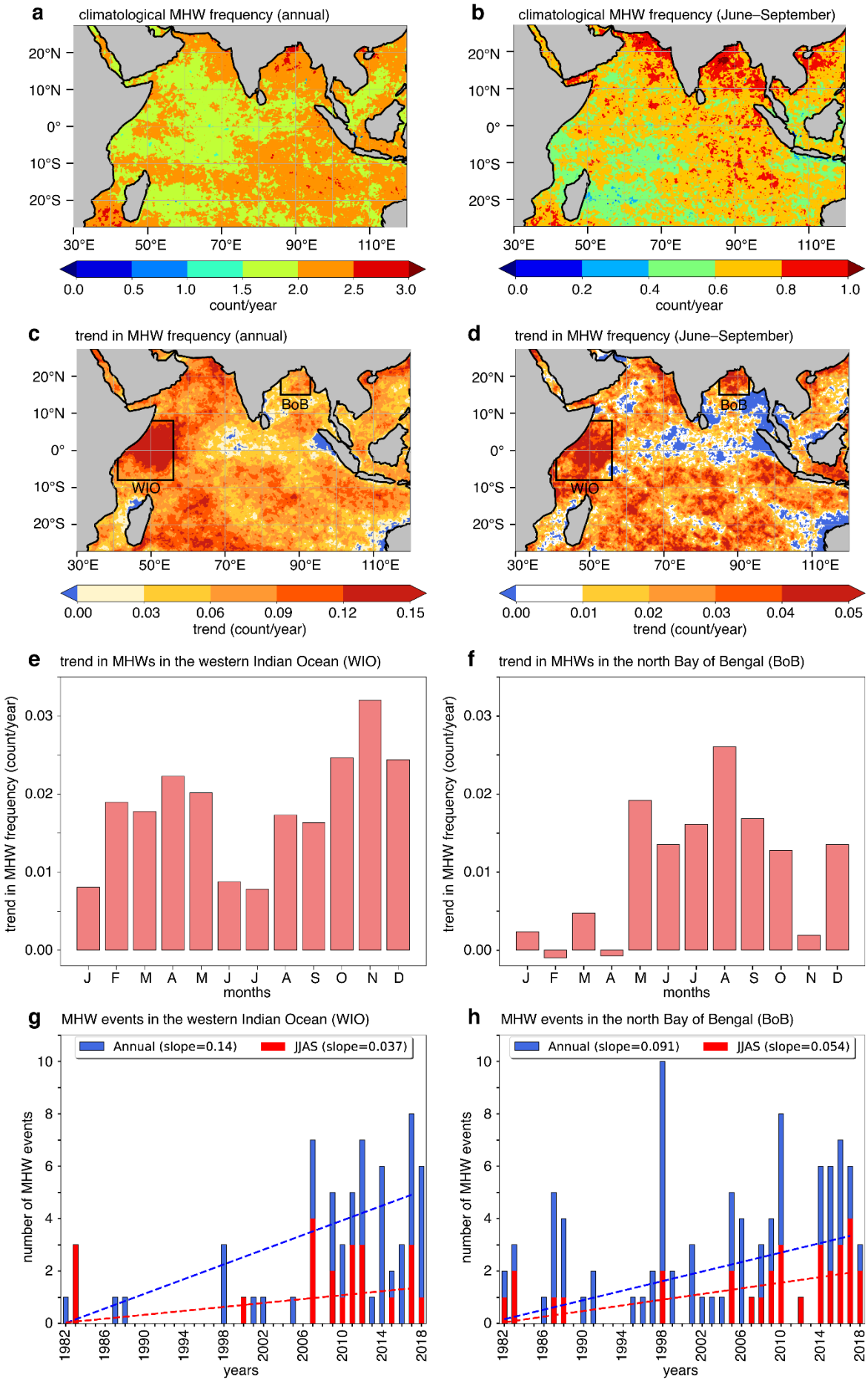
a
climatological MHW frequency (annual)
20°N
10°N
0°
10°S
20°S
30°E
50°E
70°E
90°E
110°E
0.0
0.5
1.0
1.5
2.0
2.5
3.0
count/year
b
climatological MHW frequency (June–September)
0.0
0.2
0.4
0.6
0.8
1.0
count/year
c
trend in MHW frequency (annual)
BoB
WIO
0.00
0.03
0.06
0.09
0.12
0.15
trend (count/year)
d
trend in MHW frequency (June–September)
0.00
0.01
0.02
0.03
0.04
0.05
trend (count/year)
e
trend in MHWs in the western Indian Ocean (WIO)
trend in MHW frequency (count/year)
J
F
M
A
M
J
J
A
S
O
N
D
months
f
trend in MHWs in the north Bay of Bengal (BoB)
g
MHW events in the western Indian Ocean (WIO)
Annual (slope=0.14)
JJAS (slope=0.037)
number of MHW events
1982
1986
1990
1994
1998
2002
2006
2010
2014
2018
years
h
MHW events in the north Bay of Bengal (BoB)
Annual (slope=0.091)
JJAS (slope=0.054)

690

691 **Figure 1:** Climatology and trend in MHW frequency (count/year) in the Indian Ocean during
692 1982–2018 (a, c) annually and for (b, d) June–September, using NOAA OISST data. Month-
693 wise trend of MHW frequency in the (e) western Indian Ocean (WIO, 41°E–56°E, 8°S–8°N)
694 and (f) north Bay of Bengal (85°E–93°E, 15°N–23°N). Time series of the number of MHW
695 days annually (blue bars), and during June–September (red bars), from 1982–2018 in (g) the
696 western Indian Ocean and (h) the north Bay of Bengal region. Trend lines in the figure are
697 statistically significant (p<0.05).

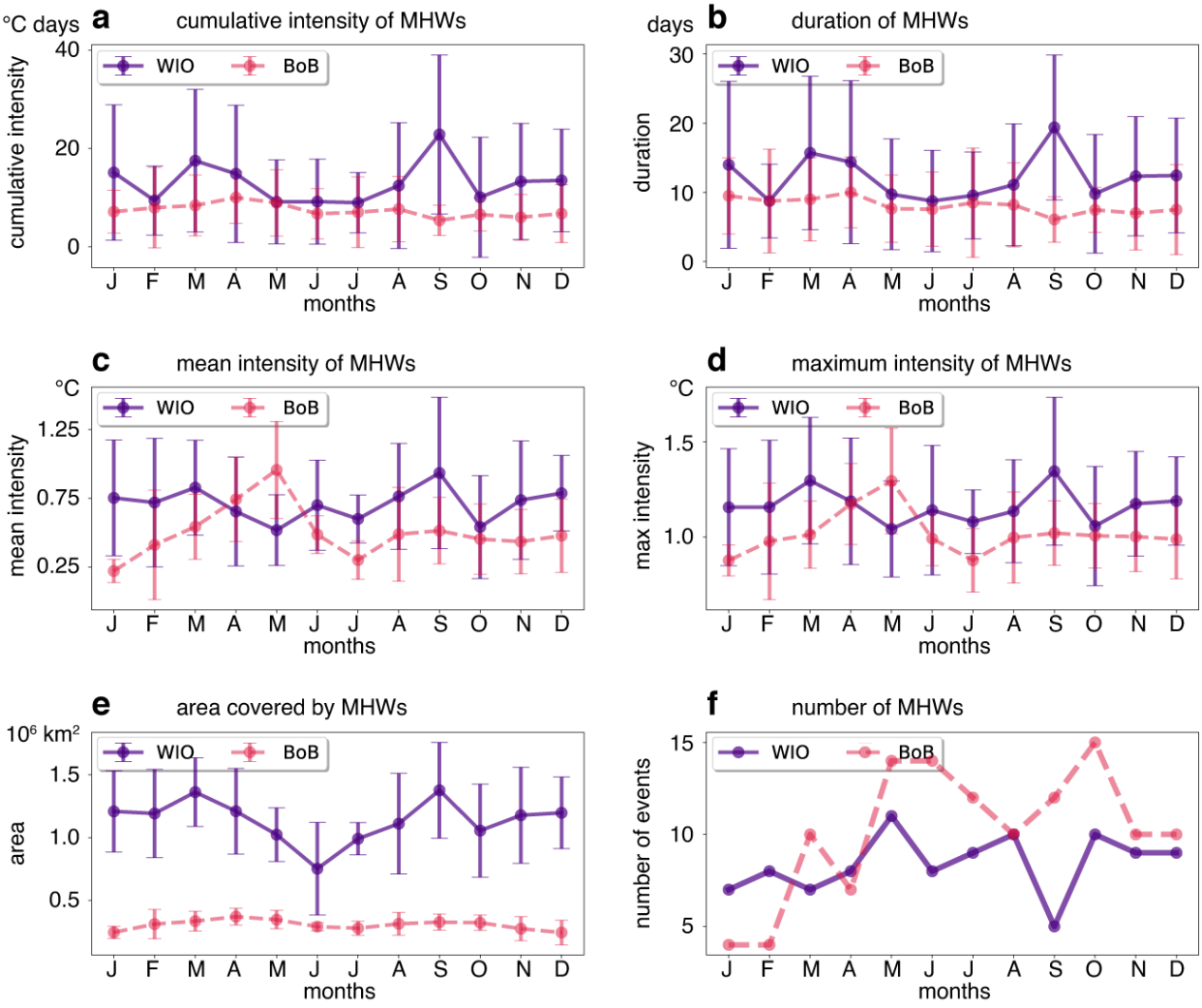

Figure 2: Month-wise climatology of MHWs. Month-wise distribution of (a) cumulative intensity (°C days), (b) mean intensity (°C), (c) duration (days), (d) maximum intensity (°C), (e) area (km^2) and (f) the number of MHW events (month-wise sample size of MHWs, based on which the month-wise climatology is estimated), during 1982–2018 for the western Indian Ocean (WIO, 41°E–56°E, 8°S–8°N) and the north Bay of Bengal (BoB, 85°E–93°E, 15°S–23°N). The error bar represents the standard deviation.

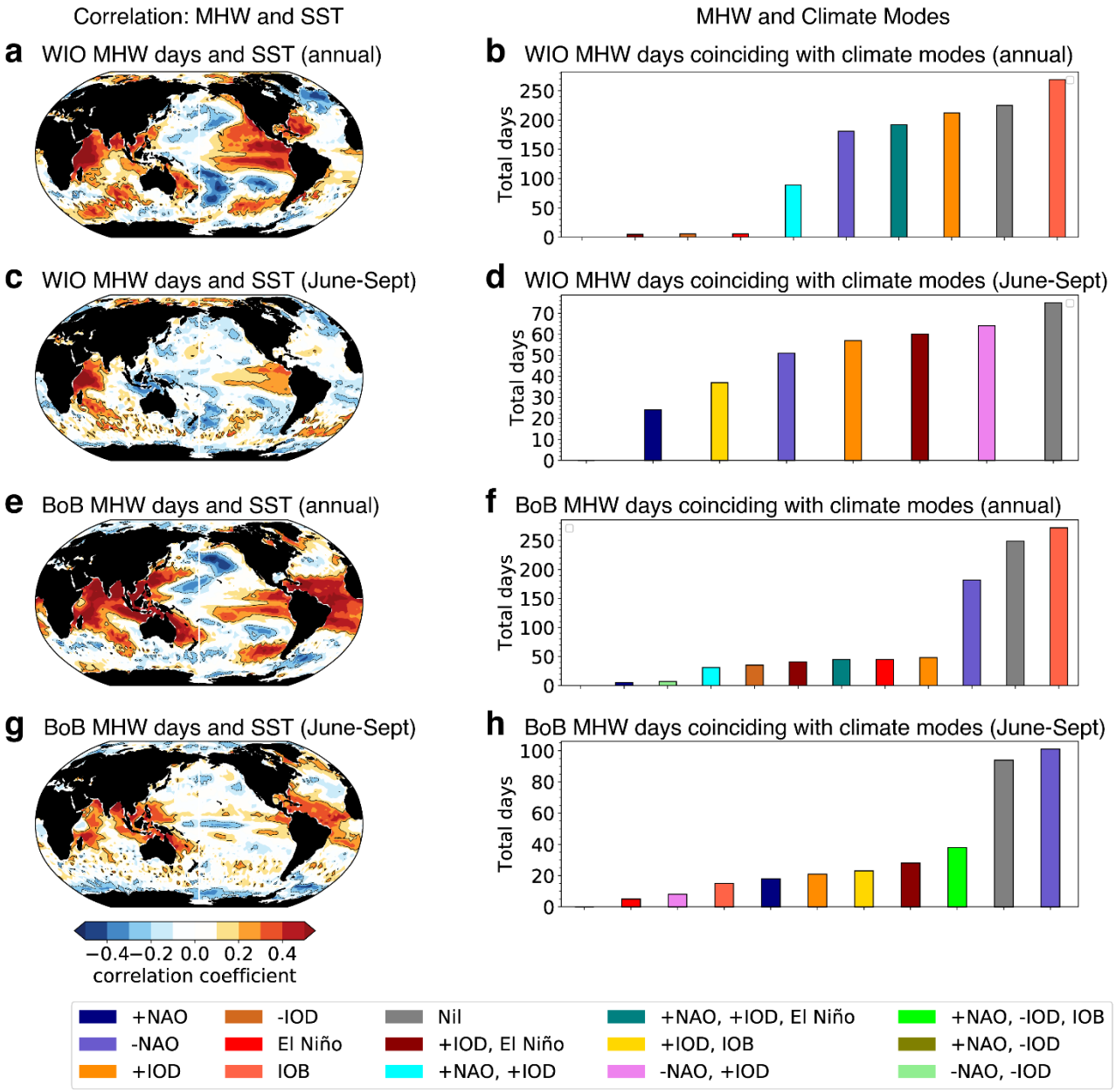

Figure 3: Correlation between the total number of MHWs and global SST for (a, e) annual and (c, g) June to September in the western Indian Ocean (WIO) and the north Bay of Bengal (BoB). The bar-charts (b, d, f, h) indicate the total number of MHW days coinciding with climate modes. "Nil" means the MHW days that do not coincide with any of the climate modes. MHW days during co-occurring climate modes are not counted for individual modes.

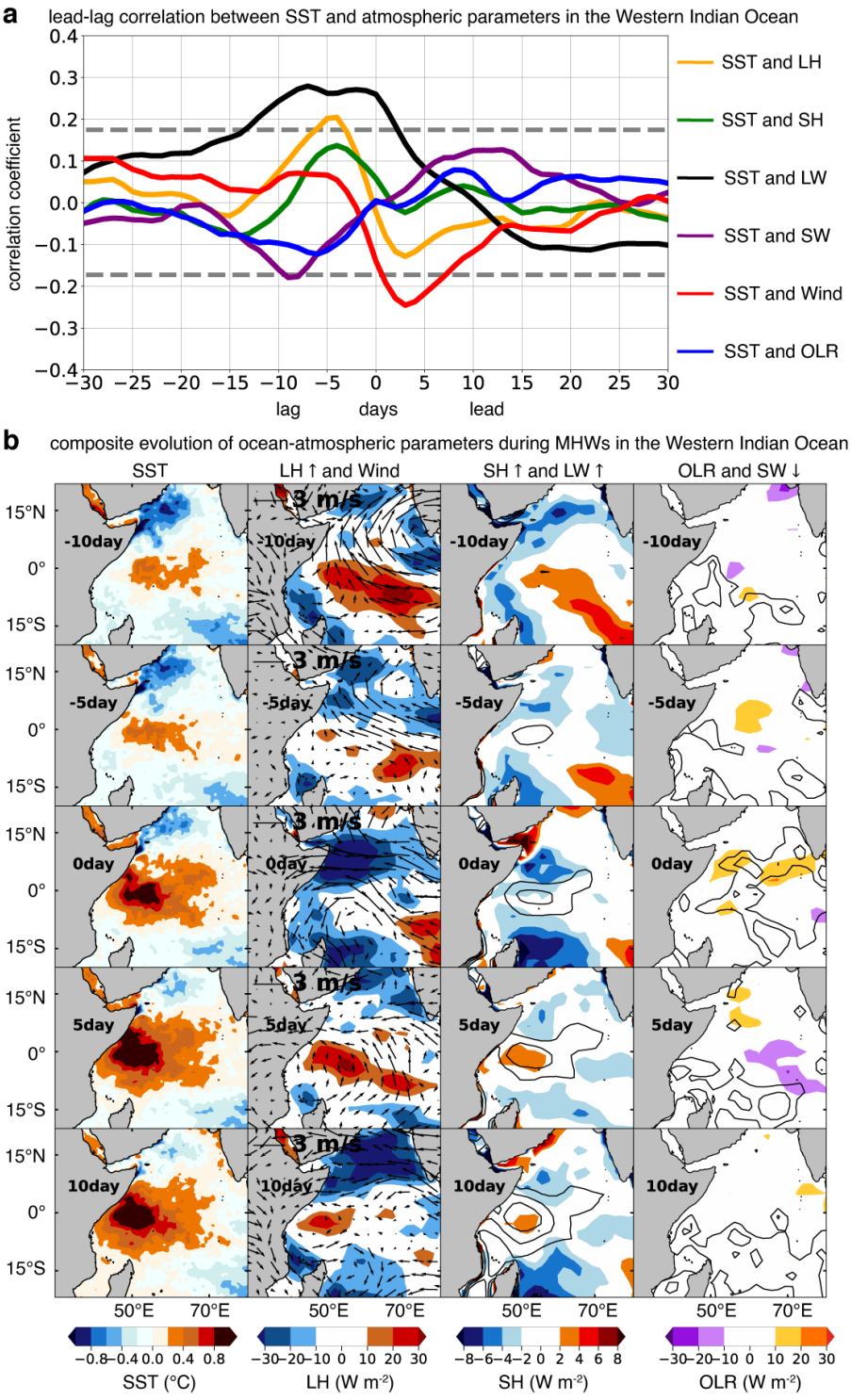

Figure 4: (a) The lead-lag correlation between SST and wind speed (red line), latent heat flux (orange line), sensible heat flux (green line), upward long wave radiation (black line), OLR (blue line) in the western Indian Ocean, estimated from the 30 days before and 30 days after the genesis of MHW events. The dotted lines represent the correlation significant at 95% confidence level based on a student's *t*-test. Composite evolution of (b) SST (°C), latent heat (LH, W m^{-2}), wind (m s^{-1}), OLR (W m^{-2}), shortwave radiation (SW, W m^{-2}), sensible heat (SH, W m^{-2}), and longwave (LW, W m^{-2}), in the western Indian Ocean before and during MHWs for the period 1982–2018, using

719 NCEP/NCAR reanalysis datasets. Upward arrow represents the exchange of flux from ocean to
720 atmosphere and downward arrow represents the exchange of flux from ocean to atmosphere.

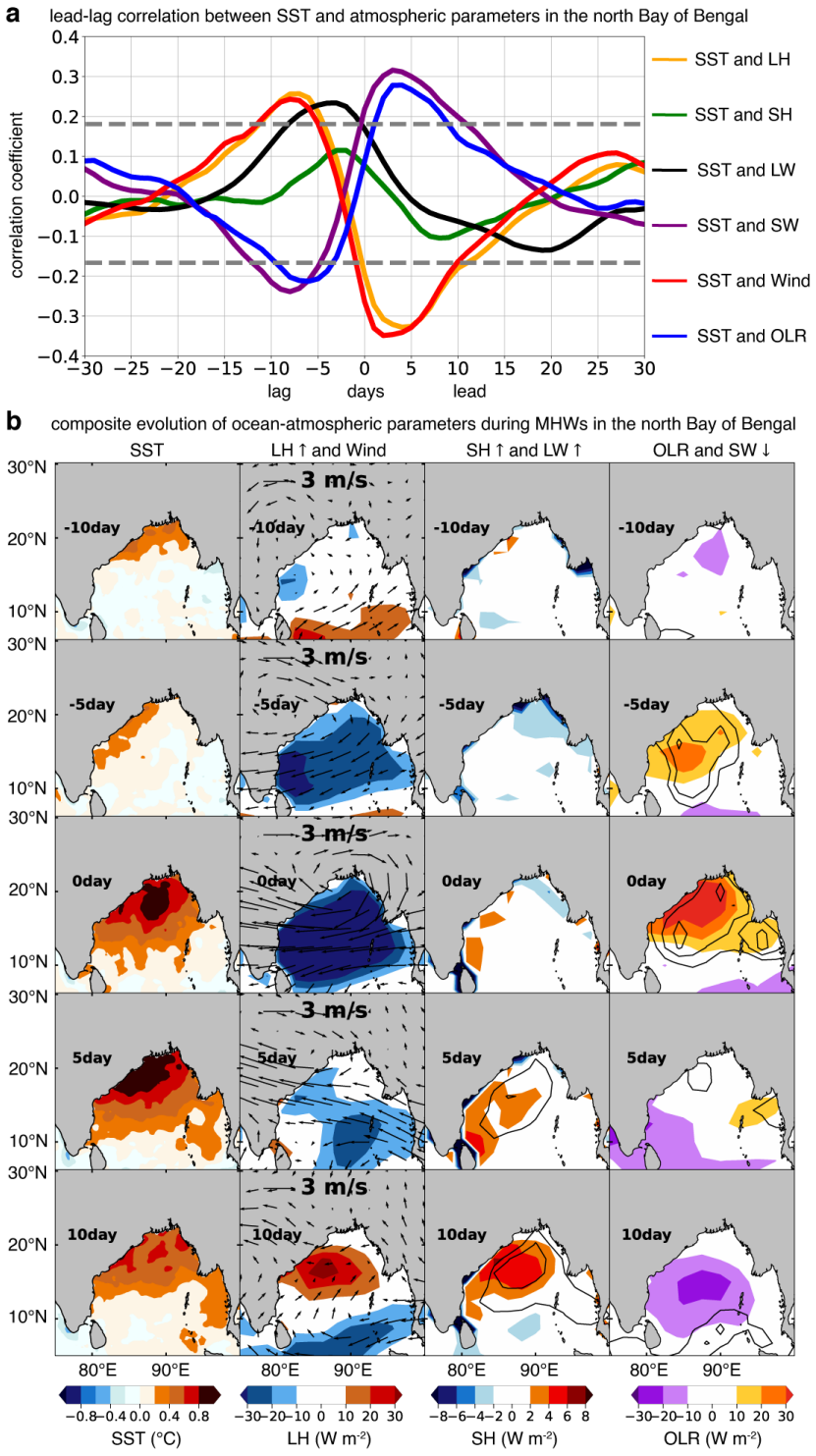

721

722 **Figure 5:** (a) The lead-lag correlation between SST and wind speed (red line), latent heat flux
723 (orange line), sensible heat flux (green line), upward long wave radiation (black line), OLR (blue
724 line) in the north Bay of Bengal, estimated from the 30 days before and 30 days after the genesis
725 of MHW events. The dotted lines represent the correlation significant at 95% confidence level
726 based on a student's *t*-test. Composite evolution of (b) SST (°C), latent heat (LH, W m^{-2}), wind (m
727 s^{-1}), OLR (W m^{-2}), shortwave radiation (SW, W m^{-2}), sensible heat (SH, W m^{-2}), and longwave (LW,
728 W m^{-2}), in the western Indian Ocean before and during MHWs for the period 1982–2018, using

729 NCEP/NCAR reanalysis datasets. Upward arrow represents the exchange of flux from ocean to
730 atmosphere and downward arrow represents the exchange of flux from ocean to atmosphere.

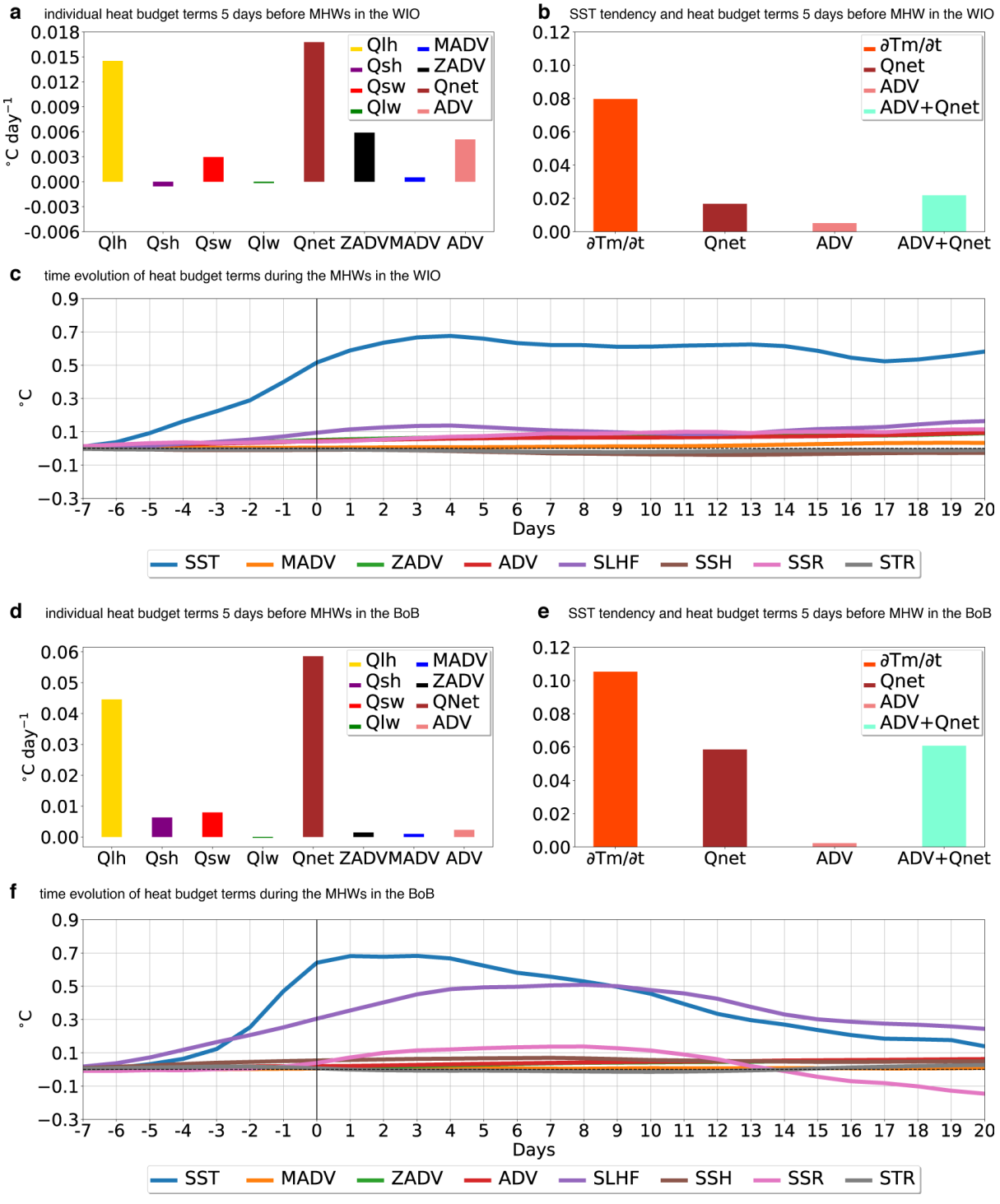

731

732 **Figure 6:** (a, d) Individual heat-budget terms (in °C day^{-1}) and (b, e) SST tendency with the heat
733 budget terms 5 days before the genesis of MHW in the western Indian Ocean (WIO) and the north
734 Bay of Bengal (BoB). (c, f) Time evolution of the heat budget terms (in °C) during the evolution
735 of MHWs in the WIO and BoB. Heat budget terms estimated using the OSCAR current data and
736 NCEP/NCAR fluxes during 1994–2015.

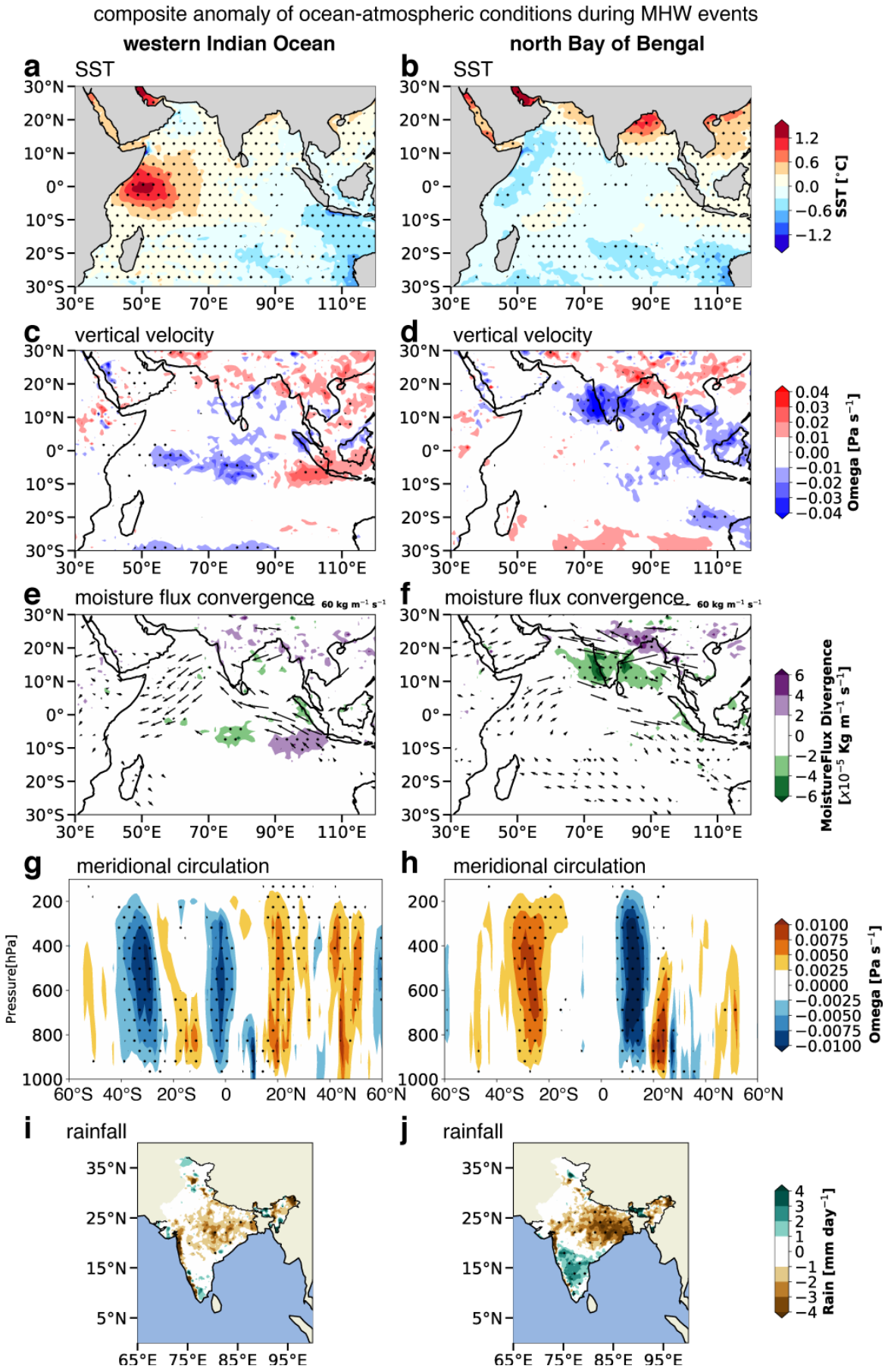
composite anomaly of ocean-atmospheric conditions during MHW events
western Indian Ocean
north Bay of Bengal
a SST
b SST
c vertical velocity
d vertical velocity
e moisture flux convergence
f moisture flux convergence
g meridional circulation
h meridional circulation
i rainfall
j rainfall
SST [°C]
Omega [Pa s⁻¹]
MoistureFlux Divergence [x10⁻⁵ Kg m⁻¹ s⁻¹]
Pressure[hPa]
Rain [mm day⁻¹]

738 **Figure 7:** Composite anomaly of daily (a, b) sea surface temperature anomalies (SST, °C), (c, d)
739 vertical velocity anomalies (omega at 500 hPa, Pa s^{-1}), (e, f) moisture flux convergence (kg m^{-1} s^{-1}),
740 (g, h) meridional circulation over 41°E–100°E (vertical velocity, Pa s^{-1}) and (i, j) rainfall (mm
741 day^{-1}) during MHW days in the western Indian Ocean and north Bay of Bengal, during June–
742 September, for 1982–2018. Stippling (black dots) indicates anomaly values significant at 95%
743 confidence level.

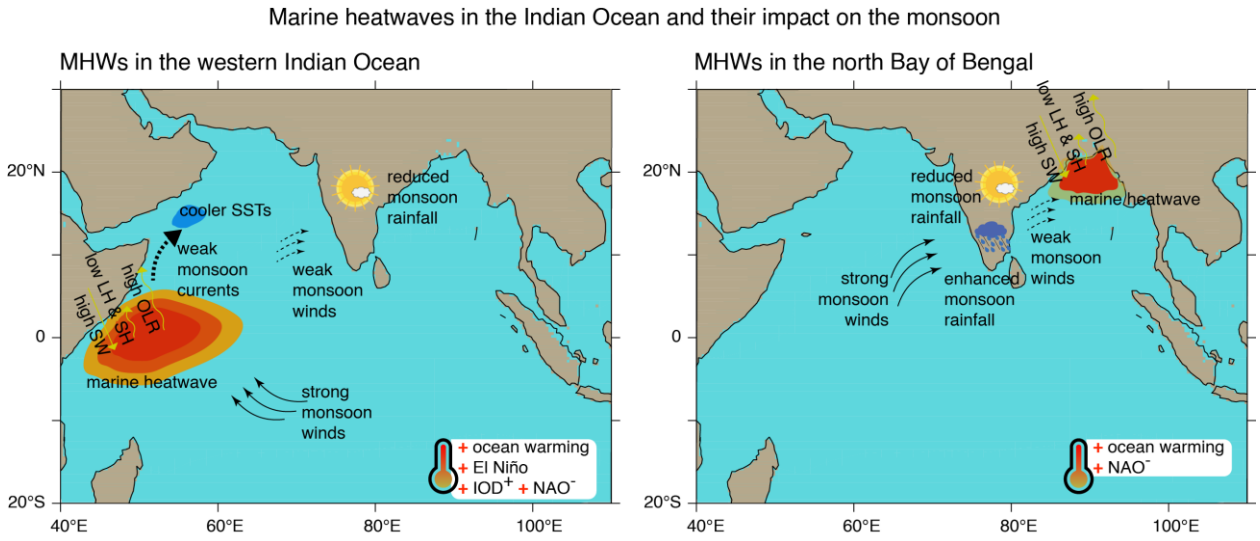

744

745 **Figure 8:** Schematic diagram depicting the factors leading to the genesis of MHW in (a) the
746 western Indian Ocean and (b) the north Bay of Bengal, and its impact on the Indian summer
747 monsoon rainfall. The legend alongside the thermometer indicates the association with ocean
748 warming and various climate modes.